# Hybrid geodesic region-based curve evolutions for image segmentation

Shawn Lankton[a], Delphine Nain[b], Anthony Yezzi[a], and Allen Tannenbaum[a]

[a]Department of Electrical and Computer Engineering, Georgia Institute of Technology, Atlanta GA 30332, USA

[b]Department of Computing, Georgia Institute of Technology, Atlanta GA 30332, USA

## ABSTRACT

In this paper we present a gradient descent flow based on a novel energy functional that is capable of producing robust and accurate segmentations of medical images. This flow is a hybridization of local geodesic active contours and more global region-based active contours. The combination of these two methods allows curves deforming under this energy to find only significant local minima and delineate object borders despite noise, poor edge information, and heterogeneous intensity profiles. To accomplish this, we construct a cost function that is evaluated along the evolving curve. In this cost, the value at each point on the curve is based on the analysis of interior and exterior means in a local neighborhood around that point. We also demonstrate a novel mathematical derivation used to implement this and other similar flows. Results for this algorithm are compared to standard techniques using medical and synthetic images to demonstrate the proposed method's robustness and accuracy as compared to both edge-based and region-based alone.

**Keywords:** Algorithms

## 1. INTRODUCTION

Segmentation is an important tool in medical image processing. It allows clinicians to visualize organs and structures in the body, analyze the shapes and sizes of these objects, and diagnose pathologies more quickly and accurately. We originally developed this algorithm in order to segment sub-cortical structures in MRI images.[1] Segmentation is required as a first step to shape analysis and other medical research objectives. Specifically, we developed and tested this algorithm to segment MRI images of the putamen.

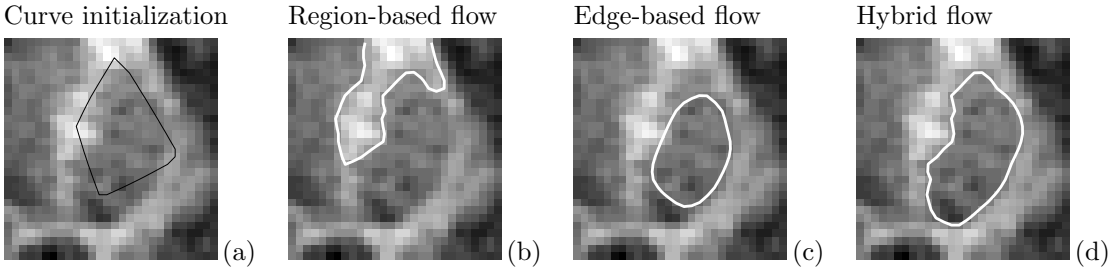


**Figure 1.** A 2D slice of a 3D MRI image of the putamen being segmented by several methods. (a) The initial contour. (b) Attempted segmentation using the Chan-Vese region-based active contour. (c) Attempted segmentation using edge-based geodesic active contours. (d) Correct segmentation using the presented hybrid flow.

Sub-cortical structures such as the putamen seen in Figure 1 pose an interesting problem because they lack a homogeneous intensity profile making it hard to characterize the statistics of the object globally. Furthermore, their poor edge definition and close proximity to other brain structures with stronger edge gradients make these

Further author information: (Send correspondence to :)
Shawn Lankton : E-mail: slankton@ece.gatech.edu, Delphine Nain : delfin@cc.gatech.edu, Anthony Yezzi : anthony.yezzi@ece.gatech.edu, Allen Tannenbaum : tannenba@ece.gatech.edu

Medical Imaging 2007: Physics of Medical Imaging, edited by Jiang Hsieh, Michael J. Flynn,
Proc. of SPIE Vol. 6510, 65104U, (2007) · 1605-7422/07/$18 · doi: 10.1117/12.709700

structures difficult to segment using standard active contour models. The purpose of this work was to develop a novel segmentation technique that can accurately identify object boundaries with robustness to image noise, and reduced dependence on initial curve placement.

In Section 2 we introduce and discuss geodesic and region based active contours to give a background on the methods that our algorithm hybridizes. Section 3 reveals the proposed hybrid energy and explains how and why it works. Information on numerical implementation and techniques used for efficient computation are shown in Section 4. Section 5 includes results on synthetic and medical images and compares them with standard geodesic and region based flows to show the improvements afforded by this algorithm. Finally, we offer concluding remarks and discuss the benefits, drawbacks, and potential for future work in Section 6. Appendix A contains the derivation of the curve flow from the proposed energy functional.

## 2. RELATED EVOLUTIONS

This section provides a brief introduction to two standard active contour segmentation techniques that the presented method both draws from and improves upon. Active contour methods begin with an initial curve and define some energy for that curve based on its geometric properties and the associated image data. Energy based on the geometry is provided to keep the curve smooth, and energies based on the image data are intended to attract the contour to object boundaries. This curve is then deformed in order to increase or decrease that energy thus moving the curve toward a local maxima or minima. Presumably this occurs when the curve is correctly situated on the object.

### 2.1. Geodesic Active Contours

Geodesic active contours take the standard active contour and reformulate the problem into finding local minimum cost curves on a conformally Euclidean metric.[2,3] The key assumption here is that on the boundary of an object, there will be a strong image gradient. One benefit of this approach is that it introduces a parameterization of the curve based on its intrinsic geometric properties. By using the Euclidian arc length parameter $s$ to parameterize the evolving contour, the parameterization becomes intrinsic to the curve. The result is that the energy is necessarily dependent on the length, and therefore smoothness of the curve without the need to include an additional, separate regularizing term. In the classical definition, the energy of the curve $E$ is given by the following function where $C$ represents the evolving curve, and $I$ represents the image data

$$E = \oint_{C(s)} f(I) ds \tag{1}$$

Here, $f$ is any positive, decreasing function of the image data. Its values form the metric over which the minimum length geodesic will be found as the curve is deformed. One simple option for $f$ used in this paper for comparisons in Section 5 is the following where $\nabla \hat{I}$ denotes the spatial gradient of a Gaussian smoothed version of $I$.

$$f = \frac{1}{1 + \|\nabla \hat{I}\|^2}$$

Despite the nice properties of this method, there are some drawbacks. The energy only examines image data immediately on the curve, i.e., it is very local. This means that unless the curve is initialized very close to the desired boundary, it is likely that some insignificant local minima will be found before reaching the desired segmentation result. Additionally, the external portion of this energy depends only on the gradient of $I$ which is prone to noise. In order to keep $\nabla I$ somewhat regular, $I$ must be smoothed a great deal. This intensive smoothing of the image means that some image information is thrown out during the segmentation process and fine detail is lost.

### 2.2. Region Based Active Contours

Another approach to defining contour energies is to look at regional properties. The key assumption here is that when the curve is placed on the object border the image will be partitioned into two or more distinctive regions whose properties are easily characterized. These types of contours includes famous flows such those based on the Mumford-Shah paradigm,[4] e.g., Chan-Vese.[5] Specifically, the energy to be minimized in the Chan-Vese model is as follows where $\Omega$ and $\overline{\Omega}$ represent the interior and exterior of the curve, and $u$ and $v$ represent the mean image intensities over $\Omega$ and $\overline{\Omega}$ respectively:

$$E = \int_{\Omega} (I-u)^2 dA + \int_{\overline{\Omega}} (I-v)^2 dA \tag{2}$$

This energy is minimized when the mean image intensities in $\Omega$ and $\overline{\Omega}$ are the most accurately approximated by $u$ and $v$. This energy remains robust to image noise with no image smoothing because it looks at integrals of image data rather than image derivatives. It is also robust to initial curve placement because although the curve moves locally, it inspects global image statistics rather than just looking along the curve. As a result, the curve can move very far from its initialization to find a energy minima. While these are fantastic properties for a flow to posses, they can also be a hindrance. For instance it is often the case that the object to be segmented, the background, or both are not described accurately by mean intensities. This can lead to poor or incorrect segmentations.

## 3. HYBRID EVOLUTION

The hybrid energy in this paper aims to blend the benefits of the geodesic active contours and the region based active contours. This is accomplished by forming a geodesic energy from local regions around the curve. The resulting flow is more robust to initial curve placement and image noise like region-based flows, but also capable of finding significant local minima and partitioning the image without making global assumptions about its makeup. The key assumption that we make about objects to be segmented by this technique is this: At each point on the true edge of an object, nearby points inside and outside the object will be modeled well by the mean intensities of the local regions. The result is an energy that is more global in nature than edge-based flows.

### 3.1. Energy Definition

We begin with the geodesic energy presented in Equation (1). However, in this formulation we must choose our $f$ such that it will be smallest when our key assumption is met. The $f$ we choose makes use of image data over local regions thus making it similar to the region-based flows described above. Here again, $\Omega$ and $\overline{\Omega}$ represent the region on the interior and exterior of the curve respectively.

$$E = \oint_{C(s)} \int_{x\in\Omega} (I\chi(x,s) - u_\ell(s))^2 + \int_{x\in\overline{\Omega}} (I\chi(x,s) - v_\ell(s))^2 \, ds \tag{3}$$

Recall that $s$ parameterizes the curve and hence specifies every point along it as the contour integral is evaluated. In this hybrid energy, $u_\ell(s)$ and $v_\ell(s)$ are the arithmetic means of points in local neighborhoods around the point $C(s)$. These neighborhoods are defined by a characteristic function $\chi$ and the position of the curve. The $\chi$ function evaluates as 1 in a local neighborhood defined by a small radius and 0 elsewhere. The contour then divides the region selected by $\chi$ into interior local points and exterior local points. These local neighborhoods are illustrated in Figure 2. The local means are specified in terms of $S_{I_\ell}(s)$, $S_{E_\ell}(s)$, $A_{I_\ell}(s)$, and $A_{E_\ell}(s)$ which represent the local interior and exterior sums of image intensities, and the area of local interior and exterior regions.

$$u_\ell(s) = \frac{S_{I_\ell}(s)}{A_{I_\ell}(s)} \qquad v_\ell(s) = \frac{S_{E_\ell}(s)}{A_{E_\ell}(s)} \tag{4}$$

$$S_{I_\ell}(s) = \int_{x\in\Omega} I\chi(x,s)dA \qquad S_{E_\ell}(s) = \int_{x\in\overline{\Omega}} I\chi(x,s)dA \tag{5}$$

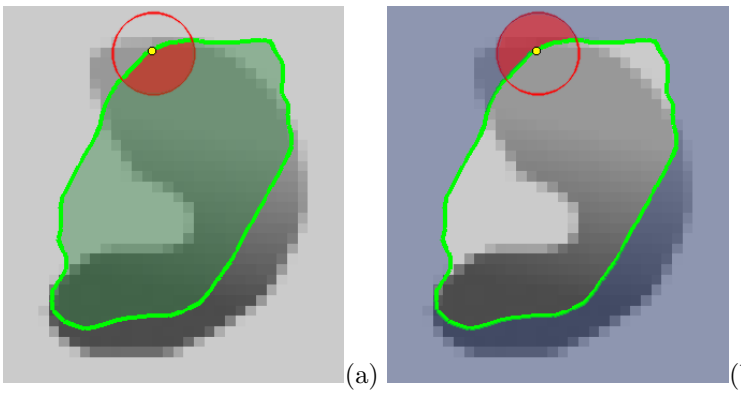

**Figure 2.** Diagrams showing local regions. Here, the circle represents the $\chi$ neighborhood. (a) Shows the region specified by $\Omega \cap \chi(x,s)$ as the shaded part of the circle. (b) Shows the region specified by $\overline{\Omega} \cap \chi(x,s)$ as the shaded part of the circle. These local regions are analyzed for every point along the curve.

$$A_{I_\ell}(s) = \int_{x \in \Omega} \chi(x,s) dA \qquad A_{E_\ell}(s) = \int_{x \in \overline{\Omega}} \chi(x,s) dA \tag{6}$$

The $\chi(x,s)$ function is a characteristic that evaluates as 1 when a point $x$ is inside of a ball $B(C(s))$ centered about the point on the curve $C$ specified by $s$ and 0 otherwise. A third parameter of the $\chi$ function is the radius of the ball represented by $B(C(s))$. This is omitted in notation as it remains constant in this implementation, and is unrelated to any parameterization of the curve.

$$\chi(x,s) = \begin{cases} 1 & x \in B(C(s)) \\ 0 & \text{otherwise} \end{cases} \tag{7}$$

### 3.2. Curve Flow

In order to deform a surface along a gradient descent such that this energy is minimized we employ variational calculus to compute the time derivative of Equation (3).[6] Computation of this derivative is not straight forward because our energy equation consists of a line integral over several region integrals. Special care was taken to ensure that all parameterizations were evaluated correctly to lead to a working curve evolution. The details of this derivation can be found in Appendix A. The resulting curve evolution is shown below.

$$\begin{aligned} C_t(s) \quad = \quad & \left( \int_{x \in \Omega} (I\chi(x,s) - u_\ell(s))^2 + \int_{x \in \overline{\Omega}} (I\chi(x,s) - v_\ell(s))^2 \right) \kappa \vec{\overline{N}} - \\ & \oint_{C(r)} \big(u_\ell(r) - v_\ell(r)\big)\big(2I\chi(x,r) - u_\ell(r) - v_\ell(r)\big) dr \vec{\overline{N}} \end{aligned} \tag{8}$$

The first thing to notice is that there are two parameters at work here: $s$ and $r$. These are both arc length parameters and $r, s \in [0 \;\; L(C)]$ where $L(C)$ is the length of the curve $C$. The first parameter, $s$ is shown as the argument to $C_t(s)$. To compute the derivative along $C$, the curve is evaluated at each point $C(s)$. At each of these points, $C$ is traversed again by a separate parameter, $r$. As $r$ traverses the curve for each point $C(s)$, the presence of the$\chi$ function centered about $C(r)$ ensures that only points in a neighborhood of $C(s)$ contribute to derivative.

The curve flow has two main terms. The first term is merely a regularizer. This is present by definition because geodesic curves will have a lower energy when they are shorter and therefore smoother. Hence, the curve moves at each point in its normal direction with a velocity proportional to its Gaussian curvature, $\kappa$ at that point. It can be shown that this is the optimal way to reduce the length of the curve as quickly as possible.[7]

Additionally, $\kappa$ is scaled by our energy evaluated at the point $C(s)$. This means that the scale is larger when the curve is not near an intensity boundary and smaller when it is. Thus as the curve approaches a boundary, the smoothing term will become less pronounced.

Now, lets look carefully at the second term. This can be positive or negative depending on the image data. This provides the direction for the curve to travel along the normal. It also becomes smaller as the curve approaches a boundary. The result is a slowing of the curve as it approaches its optimal position, and a speeding up of the curve when it is far from an optimal position. This term appears to be very similar to the derivative of the related region-based flow shown earlier in Equation( 2).

This is because the key component of both flows is the separation of regions into parts that can be modeled by their means. In Equation (2) the energy is minimized when the entire interior and exterior regions are best approximated by their means. In the presented energy in Equation (3) the energy is smallest when local regions around each point are best approximated by their means. This imposes much weaker assumptions about the composition of the image, and allows the flow to be more useful in some real-world applications.

## 4. IMPLEMENTATION

We chose to implement the minimization flow of this energy in a level-set framework in the standard way.[8,9] This is a well established tool for active contour implementations in which a signed distance function $\psi$ is used to embed the contour $C$ by storing the curve as the zero level set of $\psi$. This was chosen because it uses an intrinsic representation with no dependence on the parameterization of the curve, and allows for changes in topology automatically.

One drawback of the hybrid flow is that it is decidedly slower than most purely edge-based or region-based flows. This is because in its simplest formulation two local averages are computed for every point $C(r)$ on the curve for every point $C(s)$. Thus, $2n^2$ local averages to be computed at every iteration where $n$ is the number of points on the curve. By making some observations it is possible to greatly reduce the computational cost.

Recall from Equation (8) that at each point $C(s)$ along the curve we must traverse all points $C(r)$ and compute averages of the nearby image intensities both in and outside of $C$. Because the curve is not moving as these traversals occur, we can equivalently traverse $C$ by $r$ once and store the values at each point. Therefore, when they are needed during the traversal by $s$ they are all readily available. This reduces the number of needed averaging operations to only $2n$.

Another speed up to this algorithm is to pre-compute as much information as possible regarding the local averages so that the actual averaging operation can be performed very quickly. We accomplish this by first initializing each pixel within a narrow band of the zero level set by computing $S_{Il}$, $S_{El}$, $A_{Il}$, and $A_{El}$ from Equations (5) and (6) and storing them in memory. With these values stored, $u_\ell$ and $v_\ell$ can be computed with a single divide operation regardless of the size of the $\chi$ neighborhood. Then, as $\psi$ moves and the curve moves such that a pixel shifts from the one side of the curve to another we can quickly update only the affected points. Updating points is fast because the value of the pixel that crossed the contour is added to the interior count and subtracted from the exterior count or vice versa for all neighboring pixels within $\chi$. As the curve moves and new points enter the narrow band, these points are initialized exactly as before. In this way, we make as few computations as possible when computing local averages.

## 5. EXPERIMENTS

In the following experiments, we show results on synthetic images in Figure 3 and MRI images of the putamen in Figure 4. In these results, the hybrid flow will be directly compared with the standard geodesic flow described in Section 2.1 and the standard Chan-Vese flow described in Section 2.2. The synthetic images show a special case in which these standard segmentation techniques don't work, but the proposed method works well. The medical images of the putamen demonstrate the flow's real-world applicability to medical imaging problems. In Figures 3 and 4 the same image is shown with three different curve initializations and the resulting segmentations from the different methods are compared.

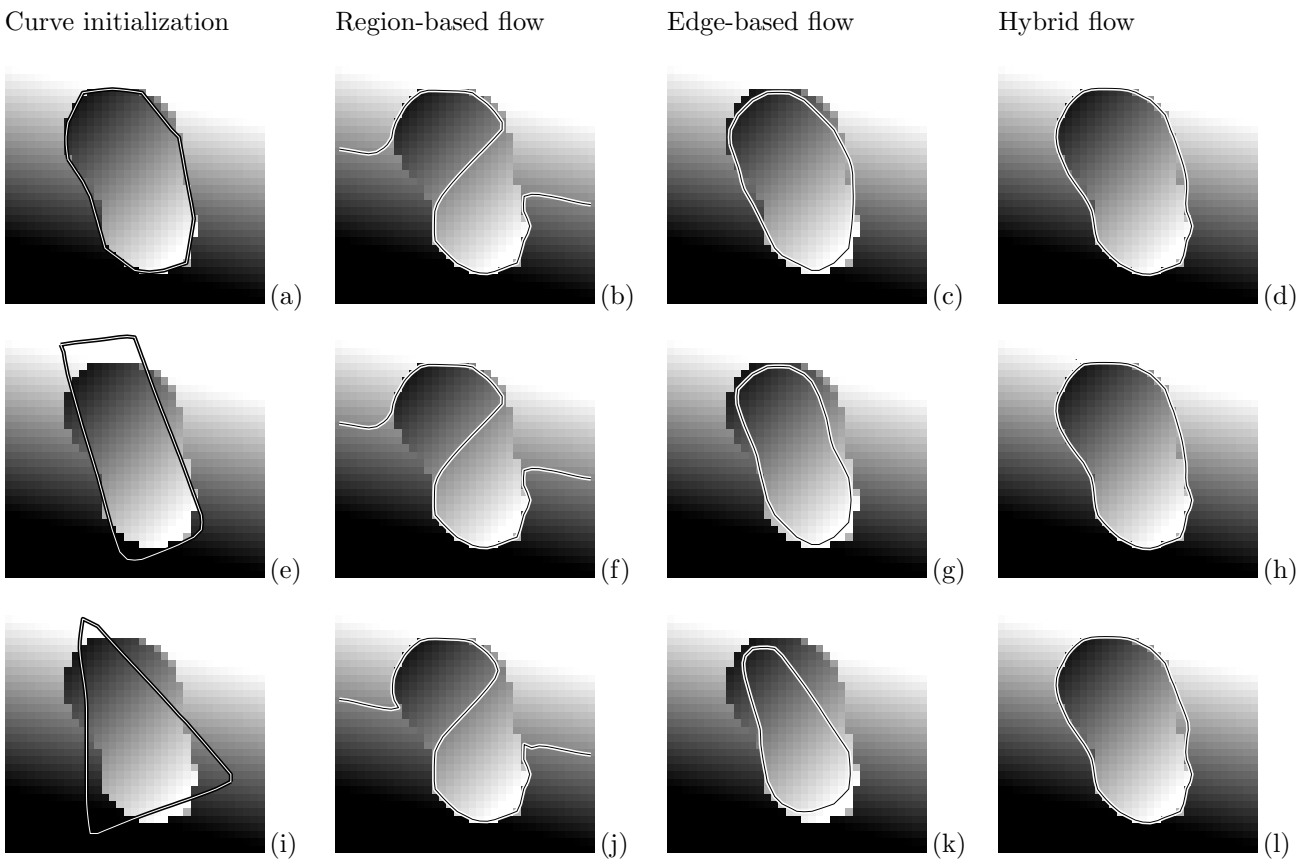


**Figure 3.** A synthetic image chosen to show the advantage of the hybrid flow being segmented by several methods. (a,e,i) The initial contours. (b,f,j) Attempted segmentations using the Chan-Vese region-based active contour. (c,g,k) Attempted segmentation using edge-based geodesic active contours. (d,h,l) Correct segmentation using the presented hybrid flow.

Notice that in Figure 3 the region-based flow is hindered by its global assumption about image composition. It finds an incorrect solution because the correct segmentation needs to be aware of local image characteristics only. The geodesic flow fails because it overemphasizes smoothness due to the Gaussian filter applied to $I$, and it misses edge information entirely if initialized too far away from the true boundary. The hybrid flow can overcome both of these problems.

Again in the medical image examples in Figure 4 we see that the Chan-Vese region-based flow finds a solution that satisfies its energy. However, because this energy isn't suited to the image, the result is not correct. Depending on the specific initialization this method finds incorrect segmentations that are either homogenous and dark or homogenous and bright. The edge-based flow is hindered by the noise in the image, and the lack of well defined edge gradients. As a result, the curve either passes the true edge without stopping, or fails to grow to find the true edge. As before, the presented hybrid flow is able to overcome these problems and achieve accurate segmentations despite the varying initialization.

## 6. DISCUSSION

The presented technique hybridizes the ideas of geodesic and region-based active contours and as a result produces a segmentation algorithm which has benefits of both. Like other geodesic models, our approach is capable of looking locally for correct solutions while only making weak assumptions about global image properties. Also, as with region based models, our method has increased robustness to noise and reduced dependence on initial curve

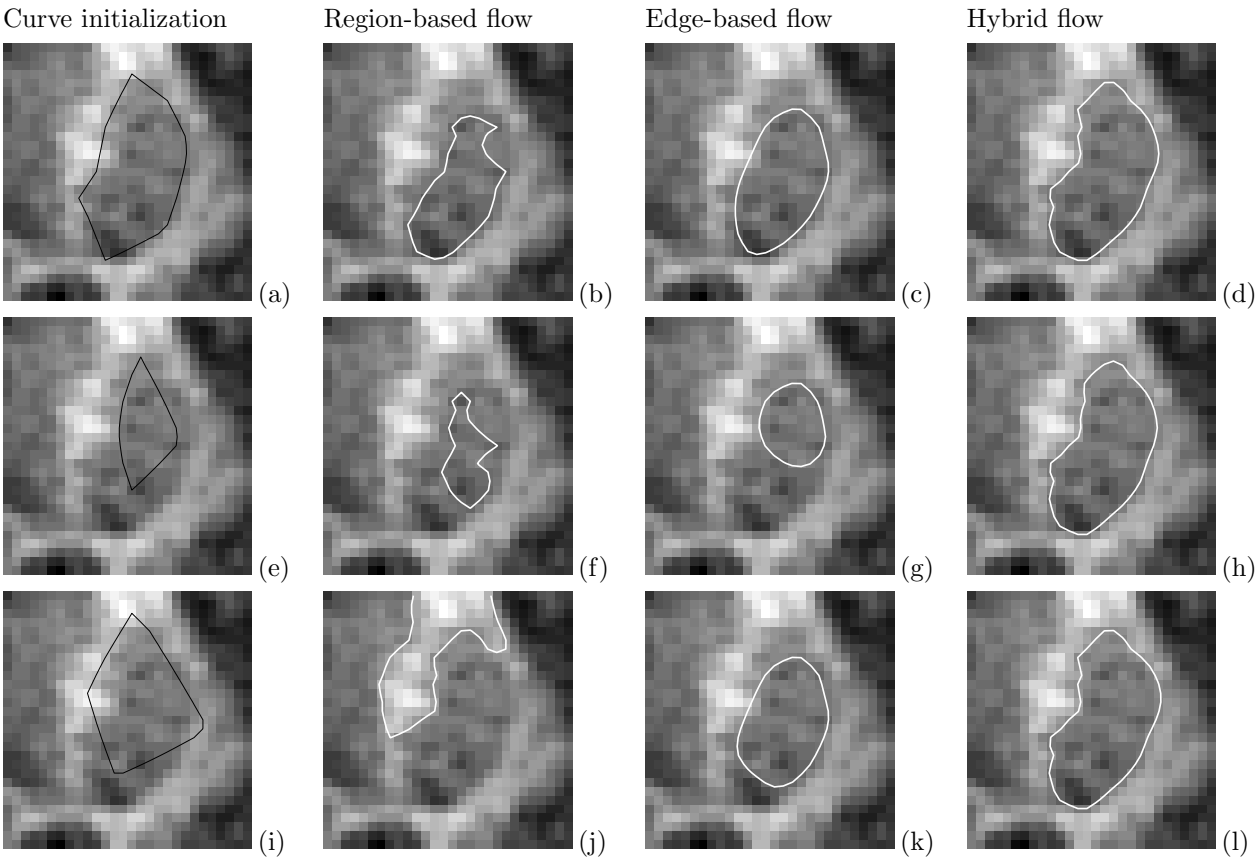


**Figure 4.** An MRI image of the putamen being segmented by several methods. (a,e,i) The initial contours. (b,f,j) Attempted segmentations using the Chan-Vese region-based active contour. (c,g,k) Attempted segmentation using edge-based geodesic active contours. (d,h,l) Correct segmentation using the presented hybrid flow.

placement as a result of taking image data from local regions. The algorithm has proven to be more versatile than either of the two standard techniques presented, even in its simplest form.

Despite its benefits, this method still has some drawbacks. As with all geometric-based energies, initial curve placement is still important. Although this algorithm is less dependent than some, it is still necessary to initialize the contour nearby the object to be segmented or risk that the final segmentation result will converge at an incorrect local minima. Additionally, the key assumption made about image makeup is not ideal for all images. There are cases where the ideal border of an object is not characterized by a separation of image intensities at that border. In these cases, our algorithm breaks down. Finally, the hidden parameter which is the size of the neighborhood defined by $\chi$ can have a significant impact on the final result. Currently this parameter must be tuned to work optimally with the types of images being used. With additional work, we hope to improve this technique and continue to explore its possibilities.

The method presented here is merely the first application of a new class of energy functionals based around combining local and global flows. The ability to define a geodesic energy with respect to local regions of image data has many possible applications. Extension of the implementation to accommodate higher order statistics, vector valued images, and images of higher dimensionality will improve performance and open the door to other potential applications.

## APPENDIX A. DERIVATION OF CURVE FLOW

In this section we will derive the curvature flow that minimizes the energy presented in Equation (3). Let us begin by recalling the energy, and re-defining it in terms of several other functions, $f(I,s)$, $g(I,s)$, and $h(I,s)$. This will make it easier to break down the derivation into simpler steps.

$$E = \oint_{C(s)} f(I,s)ds \tag{9}$$

$$f(I,s) = \int_{x\in\Omega} g(I,s)dA + \int_{x\in\overline{\Omega}} h(I,s)dA \tag{10}$$

$$g(I,s) = (I\chi(x,s) - u_\ell(s))^2 \qquad h(I,s) = (I\chi(x,s) - v_\ell(s))^2 \tag{11}$$

With these substitutions made, we can begin to take the time derivative of $E$. The first step will be to change from our implicit parameterization by the arc length parameter $s \in [0 \;\; L(C)]$ to one that is not time dependent. We will use $p \in [0 \;\; 1]$ to denote a parameter on a fixed interval. To make this change correctly we recall the definition of arc length:

$$L = \oint_0^1 \|C_p\|dp = \oint_{C(s)} ds \quad \Rightarrow \quad \|C_p\|dp = ds$$

Once the substitution from $s$ to $p$ parameters is made we can move derivatives through the contour integrals. Hence, when we take the time derivative of $E$ we can move the $\nabla_t$ inside of the integral and obtain two terms by applying the product rule to the integrand.

$$\begin{aligned}
\nabla_t E &= \nabla_t \oint_{C(s)} (f(I,s))ds \\
&= \oint_0^1 \nabla_t (f(I,p)\|C_p\|)dp \\
&= \oint_0^1 f(I,p)\|C_p\|_t dp + \oint_0^1 \nabla_t f(I,p)\|C_p\|dp
\end{aligned} \tag{12}$$

Now we will look at these terms separately. The first term is manipulated such that it is parameterized once again by $s$. As this is done, we see that this part of the derivative is dependent on curvature. This is a typical part of the result for a geodesic active contour. In these equations $\overrightarrow{T}$ represents the unit tangent, $\overrightarrow{N}$ represents the unit normal, and $\kappa$ represents the Gaussian curvature.

$$\begin{aligned}
&\oint_0^1 f(I,s)\left\langle C_{pt} \;, \overrightarrow{T}\right\rangle dp \\
&\oint_0^1 f(I,s)\left\langle C_t \;, -\overrightarrow{T}_p\right\rangle dp \\
&\oint_{C(s)} f(I,s)\left\langle C_t \;, -\kappa\overrightarrow{N}\right\rangle ds \\
&\oint_{C(s)} \left\langle C_t \;, -f(I,s)\kappa\overrightarrow{N}\right\rangle ds \\
&\oint_{C(s)} \left\langle C_t, -\left(\int_{x\in\Omega}(I\chi(x,s) - u_\ell(s))^2 + \int_{x\in\overline{\Omega}}(I\chi(x,s) - v_\ell(s))^2\right)\kappa\overrightarrow{N}\right\rangle
\end{aligned} \tag{13}$$

The second term requires more work, because here the derivative is applied to $f$. First, we rewrite $f$ in terms of $g$ and $h$. Then distributing the derivatives we see two expressions of the form $\int_\Omega g \; dA$ and $\int_{\overline{\Omega}} h \; dA$. The

derivatives of this type of functional are known provided $g$ and $h$ are only functions of the image. Thus, the solution is immediately rewritten to reflect this and like terms are combined:

$$\begin{aligned}
&\oint_0^1 \nabla_t f(I,p)\|C_p\|dp \\
&\oint_0^1 \left(\nabla_t \int_{x\in\Omega} g(I,p)\ dA + \nabla_t \int_{x\in\overline{\Omega}} h(I,p)\ dA\right)\ \|C_p\|\ dp \\
&\oint_0^1 \left(\oint_{C(s)} \left\langle C_t(s), g(I,p)\overrightarrow{N}\right\rangle dr + \oint_{C(s)} \left\langle C_t(s), h(I,p)\overrightarrow{N}\right\rangle ds\right)\|C_p\|dp \\
&\oint_0^1 \oint_{C(s)} \left\langle C_t(s), \big(g(I,p)+h(I,p)\big)\overrightarrow{N}\right\rangle dr\|C_p\|dp
\end{aligned}$$

Now that $C_t$ is isolated, we can return our outer integral to parameterization by arc length. However, because $s$ is being used in the interior integral we will use $r$ to denote a second arc length parameter evaluated separately.

$$\oint_{C(r)} \oint_{C(s)} \left\langle C_t(s), \big(g(I,r)+h(I,r)\big)\overrightarrow{N}\right\rangle ds\ dr$$

At this point, we make a key observation. Because the only terms that depend on the parameter $r$ are inside the dot product, we can move the integral over $r$ inside the dot product as well. Finally an algebraic manipulation is performed to improve readability.

$$\begin{aligned}
&\oint_{C(s)} \left\langle C_t(s), \oint_{C(r)} \big(g(I,r)+h(I,r)\big)dr\ \overrightarrow{N}\right\rangle ds \\
&\oint_{C(s)} \left\langle C_t(s), \oint_{C(r)} \Big((I\chi(x,r)-u_\ell(r))^2 - (I\chi(x,r)-v_\ell(r))^2\Big)\ dr\ \overrightarrow{N}\right\rangle ds \\
&\oint_{C(s)} \left\langle C_t(s), \oint_{C(r)} \big(u_\ell(r)-v_\ell(r)\big)\big(2I\chi(x,r)-u_\ell(r)-v_\ell(r)\big)dr\ \overrightarrow{N}\right\rangle ds
\end{aligned} \tag{14}$$

Now the Equations (13) and (14) are in the same form, so we can recombine them to form the final expression for $\nabla_t E$.

$$\begin{aligned}
\nabla_t E \ = \ \oint_{C(s)} \Bigg\langle C_t\ , -\left(\int_{x\in\Omega} (I\chi(x,s)-u_\ell(s))^2 + \int_{x\in\overline{\Omega}} (I\chi(x,s)-v_\ell(s))^2\right)\kappa\overrightarrow{N} + \\
\oint_{C(r)} \big(u_\ell(r)-v_\ell(r)\big)\big(2I\chi(x,r)-u_\ell(r)-v_\ell(r)\big)dr\ \overrightarrow{N}\Bigg\rangle ds
\end{aligned} \tag{15}$$

Finally, from here we can read the expression for curvature flow.

$$\begin{aligned}
C_t(s) \ &= \ f(I,s)\kappa\overrightarrow{N} - \oint_{C(r)} \big(g(I,r)-h(I,r)\big)\,dr\overrightarrow{N} \\
C_t(s) \ &= \ \left(\int_{x\in\Omega} (I\chi(x,s)-u_\ell(s))^2 + \int_{x\in\overline{\Omega}} (I\chi(x,s)-v_\ell(s))^2\right)\kappa\overrightarrow{N} - \\
&\quad \oint_{C(r)} \big(u_\ell(r)-v_\ell(r)\big)\big(2I\chi(x,r)-u_\ell(r)-v_\ell(r)\big)dr\overrightarrow{N}
\end{aligned} \tag{16}$$

## ACKNOWLEDGMENTS

This work is part of the National Alliance for Medical Image Computing (NAMIC), funded by the National Institutes of Health through the NIH Roadmap for Medical Research, Grant U54 EB005149. Information on the

National Centers for Biomedical Computing can be obtained from http://nihroadmap.nih.gov/bioinformatics. This work was also funded in part by grants from NSF, AFOSR, ARO, MURI, MRI-HEL as well as by a grant from NIH (NAC P41 RR-13218) through Brigham and Women's Hospital.

## REFERENCES

1. A. Toga and J. Mazziotta, *Brain Mapping: The Methods*, Acedemic Press, New York, 2002 (2nd Edition).
2. S. Kichenassamy, A. Kumar, P. Olver, A. Tannenbaum, and A. Y. Jr., "Conformal curvature flows: From phase transitions to active vision," *Archive for Rational Mechanics and Analysis* **134**(3), pp. 275–301, 1996.
3. V. Caselles, R. Kimmel, and G. Sapiro, "Geodesic active contours," *Int. J. of Computer Vision* **22**, pp. 61–79, 1997.
4. D. Mumford, "A bayesian rationale for energy functionals," in *Geometry Driven Diffusion in Computer Vision*, B. Romeny, ed., *Kluwer Academic, Dordrecht*, pp. 141–153, 1994.
5. T. Chan and L. Vese, "Active contours without edges," *IEEE Trans. on Image Processing* **10**(2), pp. 266–277, 2001.
6. G. Strang, *Introduction to Applied Mathematics*, Wellesley Cambridge Press, Massachusetts, 1996.
7. M. Grayson, "Shortening embedded curves," *The Annals of Mathematics* **129**, pp. 71–111, 1989.
8. J. Sethian, *Level Set Methods and Fast Marching Methods*, Springer, New York, (1999 2nd Edition).
9. S. Osher and R. Fedkiw, *Level Set Methods and Dynamic Implicit Surfaces*, Cambridge University Press, New York, 2003.